Insights into the electrochemical degradation of phenolic lignin model compounds in protic ionic liquid-water system

Guangyong Liu[1,2#], Qian Wang[1#], Dongxia Yan[1], Yaqin Zhang[1], Chenlu Wang[1], Shijing Liang[2], Lilong Jiang[2]*, and Hongyan He[1]*

[1] *CAS Key Laboratory of Green Process and Engineering, State Key Laboratory of Multiphase Complex Systems, Beijing Key Laboratory of Ionic Liquids Clean Process, Institute of Process Engineering, Chinese Academy of Sciences, Beijing 100190, China.*

[2] *National Engineering Research Center of Chemical Fertilizer Catalyst, School of Chemical Engineering, Fuzhou University, Fuzhou 350002, Fujian, China.*

[#] *Co-first author*

**Corresponding author (email: jll@fzu.edu.cn; hyhe@ipe.ac.cn)*

1. MD simulation methods

All simulations in this work were performed using the large-scale atomic/molecular massively parallel simulator (LAMMPS).[1] To analyze the structures and diffusion of O_2, protic ionic liquid [BSO_3Hmim][OTf], and four phenolic lignin model compounds (EP, PP, PBP, and 2-PEP) in mixed systems with different water contents, we created five simulation boxes with different compositions and the details are shown in **Table S1**. Periodic boundary condition (PBC) was applied in the x-, y- and z-directions for each box. The parameters of the bond, angle, dihedral, and non-bond interactions of [BSO_3Hmim][OTf] and the four phenolic lignin model compounds were described by the all-atom optimized potential for liquid simulations (OPLS-AA) force field,[2-4] which have been used successfully to obtain the structures and liquid properties.[5-7] The rigidly extended simple-point-charge (SPC/E) model was used to describe water molecules.[8] The SHAKE algorithm[9] was applied to O-H bonds to reduce the high-frequency vibrations. O_2 molecules in the gas phase were described by transferable potentials for phase equilibria-explicit hydrogen (TraPPE-EH) model with an additional point charge site.[10] The interactions between O_2 molecules, [BSO_3Hmim][OTf] and the four phenolic lignin model compounds mainly include electrostatic and van der Waals terms, the former of which is long-range Coulombic interaction computed by particle-particle-particle-mesh (PPPM) algorithm, and the latter one was described by the 12-6 Lennard-Jones potential. The Lorentz-Berthelot mixing rule was used to model the parameters between different atomic species, which are truncated at 1.2 nm.

In MD simulations, the time step for integrating Newtonian equations of motion was 0.5 fs, which was confirmed to ensure energy conservation. O_2, [BSO_3Hmim][OTf], H_2O, and all phenolic lignin model compounds were relaxed in an NPT ensemble for 15 ns at a temperature of T = 300 K and a pressure of P = 1.0 atm along x, y and z-direction. After equilibration of the system, the NPT ensemble was changed to the NVT at a 300 K temperature, where the temperature was controlled by Berendsen thermostat.[11] After

an equilibrium simulation of up to 2 ns, MD simulation continued to run an additional 3 ns in the NVE ensemble at 300 K to collect the data for analyzing the structural and diffusion properties. The diffusion coefficients were calculated by statistical averaging over at least 5 independent simulations.

Table S1. Numbers of studied ionic liquid [BSO_3Hmim][OTf], water, phenolic lignin model compounds (EP, PP, PBP, and 2-PEP), and O_2 in different systems.

V_{IL} : V_{water}	1:0	4:1	2:1	1:1
N_{IL}/pair	149	122	102	76
N_{water}/molecule	0	414	701	1060
N_{lignin}/molecule	10	10	10	10
N_{O_2} /molecule	9	14	12	9

The diffusion of cation and anion, oxygen, and model compounds in the electrolysis system was obtained, and the results are shown in **Fig. S1**. It can be seen from the **Fig. S1** that the diffusion of all the studied substances basically increases with the increase of water content.

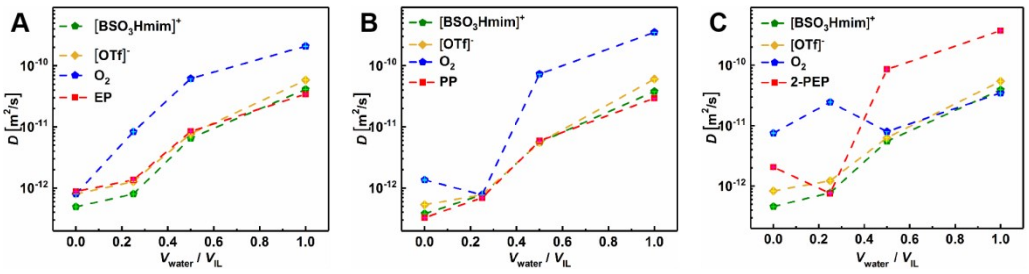

Fig S1. The diffusion coefficients of $[BSO_3Hmim]^+$, $[OTf]^-$, O_2, EP (A), PP (B) and 2-PEP (C).

2. Determining how oxygen moves

The CV curves of GC electrode in [BSO_3Hmim][OTf] or [BSO_3Hmim][OTf]-H_2O system under O_2 atmosphere at different scanning rates are shown in **Fig. S2**. The linear fitting of the peak current (I_p) to the scan rate (v) or the square root of the scan rate ($v^{1/2}$) was performed for peak ***a***. Compared with the results shown in **Fig. S2E-F**, it was demonstrated that a better linear relationship lies in I_p-$v^{1/2}$ for peak ***a*** in [BSO_3Hmim][OTf]-H_2O system than that of in pure IL, indicating that the electrode reaction process is diffusion-controlled. In other words, when a certain amount of water is added to the electrolysis system, the rate of the ORR process (peak ***a***) is controlled by the diffusion of the dissolved O_2 molecules to the working electrode surface.

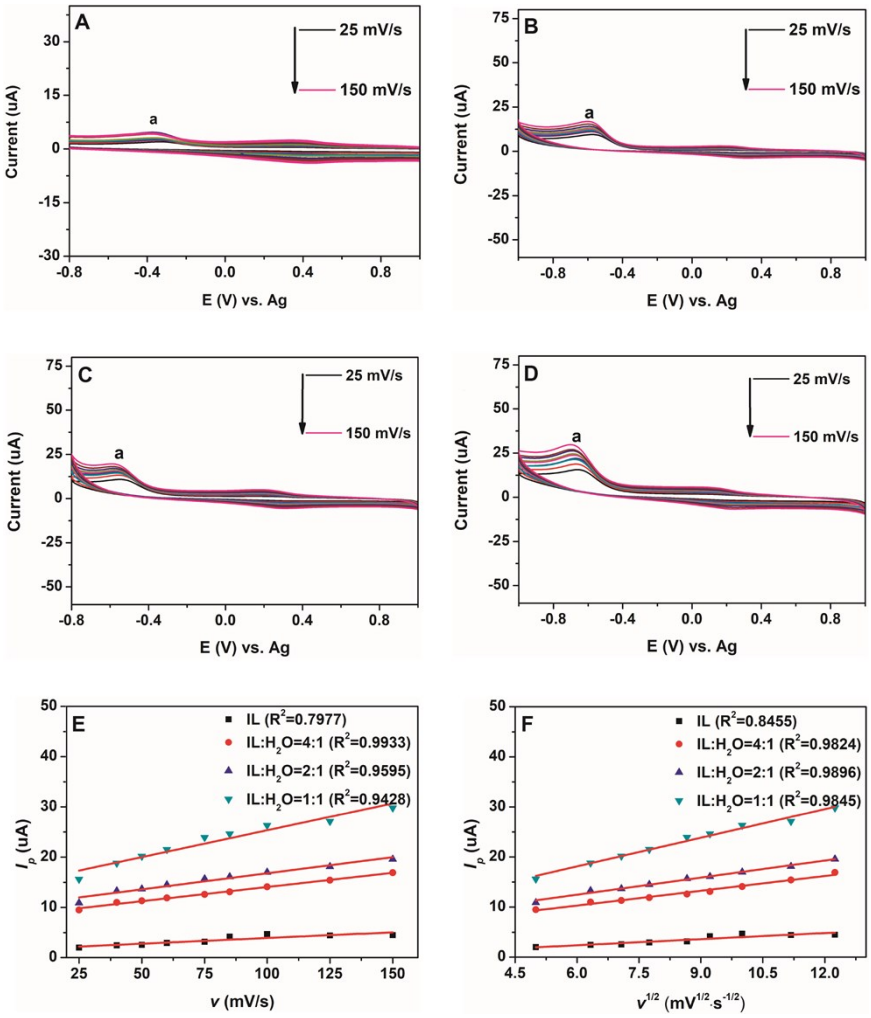

Fig S2. CV curves of GC electrode in (A) $[BSO_3Hmim][OTf]$ and $[BSO_3Hmim][OTf]$-H_2O system with volume ratio of (B) 4:1, (C) 2:1 and (D) 1:1, under O_2 atmosphere at scanning rates of 25, 40, 50, 60, 75, 85, 100, 125, 150 mV s^{-1}, respectively. (E) The linear relationship of I_p vs. v and (F) the linear relationship of I_p vs. $v^{1/2}$ for peak ***a***.

3. Redox mechanism of *p*-benzoquinone and o-hydroxyphenol

In **Fig. S3A**, when the potential was swept forward from the open circuit potential to about 1.0 V, it can be found that there is no peak in the 1st segment, a reduction peak ***e*** of *p*-benzoquinone (*p*-BQ) appears in the 2nd segment, and an oxidation peak ***f*** appears in the 3rd segment. It can be inferred that *p*-BQ is first reduced to hydroquinone (peak ***e***), and then hydroquinone is oxidized to *p*-BQ (peak ***f***). The redox mechanism of hydroquinone and *p*-BQ is shown in **Scheme S1A**. In **Fig. S3B**, when the potential was swept forward from the open circuit potential to about -1.0 V, it can be found that there is no peak in the 1st segment, an oxidation peak ***g*** of o-hydroxyphenol (o-HP) appears in the 2nd segment, and a reduction peak ***h*** appears in the 3rd segment. It can be inferred that o-HP is first oxidized to quinone (peak ***g***), and then quinone is reduced to o-HP (peak ***h***). The redox mechanism of o-HP and o-quinone is shown in **Scheme S1B**.

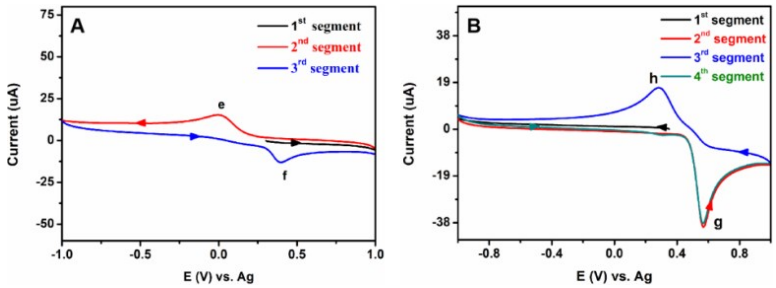

Fig S3. CV curves of GC electrode in [BSO_3Hmim][OTf]-H_2O with 1 mM *p*-BQ (A, 1:1) and 4 mM o-HP (B, 2:1) under N_2 atmosphere at a scanning rate of 50 mV s^{-1} at room temperature.

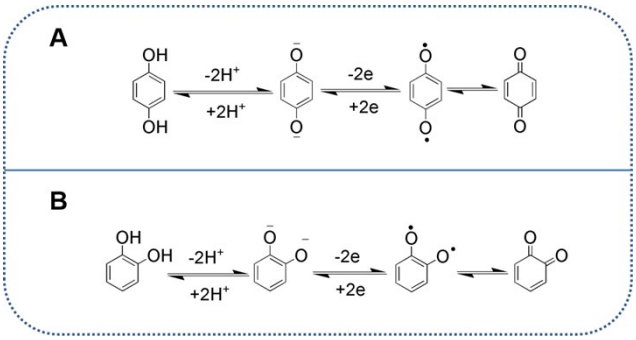

Scheme S1. Redox mechanism of *p*-BQ (A) and o-HP (B).[12]

4. Electrochemical behavior of EP, PP and 2-PEP in [BSO_3Hmim][OTf]-H_2O system

The segment-by-segment analysis of the electrochemical behavior of EP, PP and 2-PEP under N_2 atmosphere were performed, and their CV curves were very similar to that of PBP, and results are shown in **Fig. S4**. The potential was swept negatively from the open circuit potential to about -1.0 V. There is no peak in the 1st segment. Then, oxidation peaks (**1*c***, **2*c***, **2*e*** and **4*c***), and reduction peaks (**1*b***, **2*b*** and **4*b***) appear in the 2nd and 3rd segments. The CV curves of EP and 2-PEP have two oxidation peaks (**1*c*** and **1*d***, **4*c*** and **4*d***) in the 4th segment, while PP have three oxidation peaks (**2*c***, **2*d*** and **2*e***), as shown in **Fig. S4B**. We know that peaks **1*c***, **2*c*** and **4*c*** are the results of oxidation of phenolic hydroxyl groups, the reason for which has been explained in **Section 3.3** of the main text.

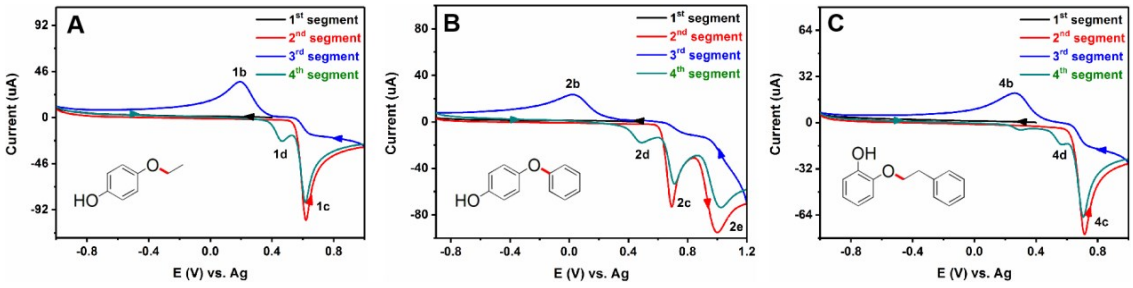

Fig S4. CV curves of GC electrode in [BSO_3Hmim][OTf]-H_2O (2:1) with 10 mM EP (A), PP (B), and 2-PEP (C) under N_2 atmosphere at a scanning rate of 50 mV s^{-1} at room temperature.

During the redox cycling, EP, PP and 2-PEP may be converted into the corresponding quinone (or hydroquinone) and hydroxyl compounds. Among them, the electrocatalytic oxidation-reduction of quinone (or hydroquinone) is relatively easy to occur, which results in the reversible conversion of quinone and hydroquinone. To confirm the speculation, we further carried out the electrochemical reduction-oxidation reaction of *p*-BQ and o-HP under N_2 atmosphere, and results are shown in **Fig. S3**. Notably, the potential of peaks **1*d***, **2*d*** and ***f*** are almost equal. So, the oxidation peaks **1*d*** and **2*d*** are related to hydroquinone oxidation (**Fig. S5A**, **B**, and **Scheme S1A**). As for the reduction peak ***e***, it overlaps with the peaks **1*b*** and **2*b***. The C-O cleavage of PP can be converted to hydroquinone and hydroxyl compounds, i.e., *p*-BQ and phenol. However, phenol also has redox properties in electrochemistry. As illustrated in **Fig. S5D**, the potential of peaks **2*e*** and ***i*** are practically equal, meaning that **2*e*** is related to phenol oxidation. As shown in **Fig. S5C** and **S3B** and **Scheme S1B**, the oxidation peak **4*d*** is related to the oxidation of o-HP.

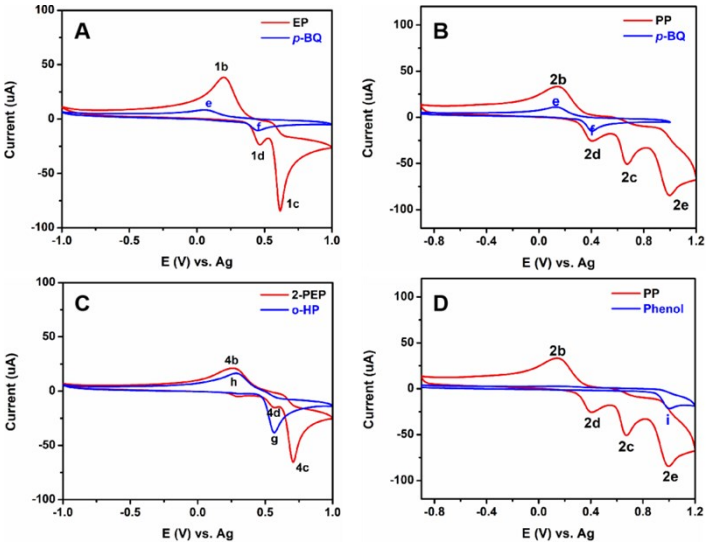

Fig S5. Comparison of GC electrode CV curves of different substrates in [BSO_3Hmim][OTf]-H_2O (2:1) under N_2 atmosphere at room temperature. Scan rate: 50 mV s^{-1}. A, B-10 mM EP and PP (red) compared with 2 mM *p*-BQ (blue). C-10 mM 2-PEP (red) compared with 4 mM o-HP (blue). D-10 mM PP (red) compared with 4 mM phenol (blue).

5. Possible redox mechanism of EP, PP, PBP, and 2-PEP

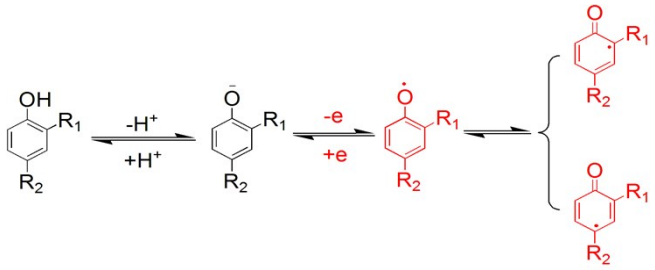

R_1=H, OH, OCH_2CH_2Ph R_2=H, OH, OCH_2CH_3, OPh

Scheme S2. Redox mechanism of EP, PP, PBP, and 2-PEP.[13,14]

6. The degradation of PBP in water, ionic liquid and ionic liquid-water systems

A comparative study of the degradation of PBP in water, ionic liquid, and ionic liquid-water systems was carried out, and the results are shown in **Fig. S6**. It can be observed that after 12 hours of electrolysis, the degradation percentage of PBP in the water system is only 4.25%, which is much lower than that of 42.54% (in [BSO_3Hmim][OTf]) and 89.08% (in [BSO_3Hmim][OTf]-H_2O (2:1)), resulting from the fact that PBP is almost insoluble in water and thus reducing the degradation of PBP. For the [BSO_3Hmim][OTf] and [BSO_3Hmim][OTf]-H_2O (2:1) systems, the addition of water leads to the decrease in the viscosity of the latter system, which facilitates the diffusion of the substrate to the electrode surface, resulting in a high degradation percentage.

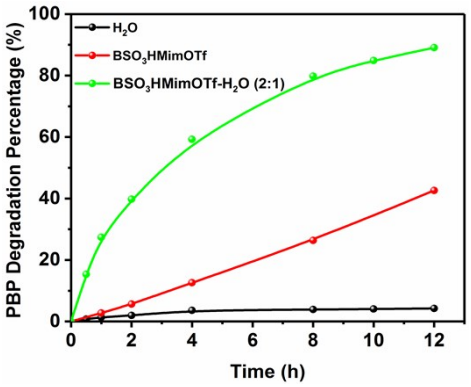

Fig S6. Degradation percentage of PBP in different systems. Blackline, H_2O; Redline, [BSO_3Hmim][OTf]; Greenline, [BSO_3Hmim][OTf]-H_2O (2:1). Conditions: RuO_2-IrO_2/Ti mesh (at 0.60 V) used as the working electrode, 20 mmol PBP, N_2 atmosphere, room temperature.

7. Kinetic investigation of PBP degradation at different working electrodes

The degradation of PBP was performed in a three-electrode cell with alternating RuO_2-IrO_2/Ti mesh (at 0.6 V) and graphite felt (at -0.6 V) as the working electrode and the other as the counter electrode. **Fig. S7** shows the kinetics of the degradation process, and it can be noticed that although the working electrodes are different, the kinetic results are similar. Comparing the data of **Fig. S7**, it can be observed that the initial rate (v_0) under O_2 atmosphere is higher than that of under N_2 atmosphere, which implies that PBP undergoes both indirect oxidation by in situ generated H_2O_2 and direct oxidation by the electrode under O_2 atmosphere, while only direct oxidation on the electrode under N_2 atmosphere. Moreover, the indirect H_2O_2 oxidation at different working electrodes is not a major contribution to the initial rate of PBP degradation, which is Δv_0=0.0119 (**Fig. S7A**) and 0.02205 mmol/(L·min) (**Fig. S7B**), respectively. Therefore, the direct oxidation of PBP on the electrode dominates the whole electrolysis process.

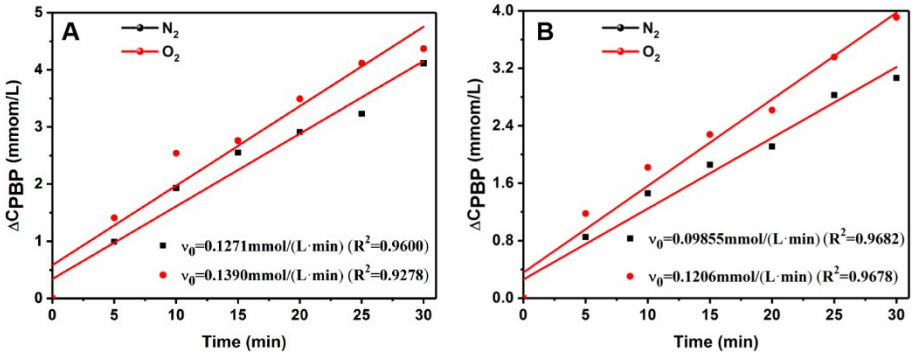

Fig S7. Kinetic study of electrocatalytic degradation of PBP at different working electrodes. (A) Graphite felt working electrode hold at -0.6 V. (B) RuO_2-IrO_2/Ti mesh working electrode hold at 0.6 V. Conditions: 20 mM PBP, room temperature, [BSO_3Hmim][OTf]-H_2O (2:1).

8. Stability of the electrolysis system

To ensure that the electrolyte does not decompose prior to substrate degradation, we verified the CV curves of the water and [BSO_3Hmim][OTf]-H_2O electrolytes before performing the degradation experiments, and the results are shown in **Fig. S8**. It is found that the CV curves of water (black line) and [BSO_3Hmim][OTf]-H_2O (red line) do not show redox peaks. Meanwhile, no bubbles are observed on the electrode surface during the reaction, which indicates that the electrolysis system is quite stable.

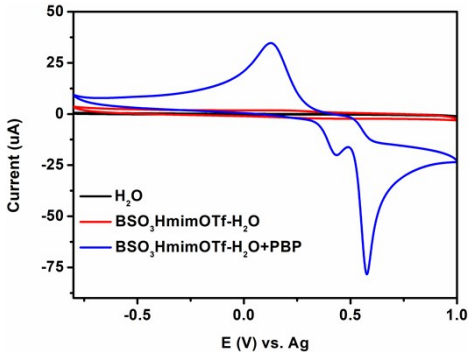

Fig S8. CV curves recorded on GC electrode under N_2 atmosphere. Deionized water (black line), [BSO_3Hmim][OTf]-H_2O (red line), [BSO_3Hmim][OTf]-H_2O+PBP (blue line).

9. Study of the chemical stability of ionic liquid

The stability of ionic liquid was investigated by constant voltage electrolysis using RuO_2-IrO_2/Ti (at 1 V) mesh as the working electrode, and the ionic liquid was characterized by Fourier transform infrared (FT-IR) spectroscopy after electrolysis. The results are shown in **Fig. S9**, wherein (A) is the FT-IR spectra of ionic liquid after 12 h electrolysis, (B) is the FT-IR spectra of ionic liquid after 4 h electrolysis, (C) is the FT-IR spectra of pure ionic liquid without electrolysis. It is found that the vibrational peaks of the FT-IR spectra are almost the same, indicating that the ionic liquids used in this experiment have preferable stability.

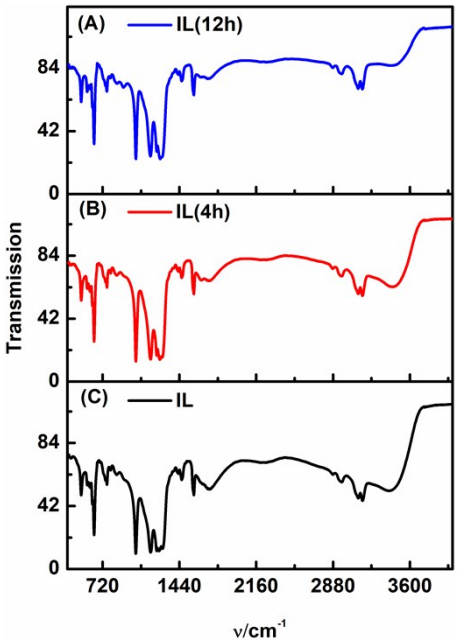

Fig S9. FT-IR spectra of IL system. (A): FT-IR spectra of ionic liquid after 12 h electrolysis, (B): FT-IR spectra of ionic liquid after 4 h electrolysis, (C): FT-IR spectra of pure ionic liquid without electrolysis.

10. Chromatograms EP, PP, PBP and 2-PEP in [BSO_3Hmim][OTf]-H_2O (2:1) electrolyte

Fig. S10 shows the HPLC chromatograms of the four lignin model compounds studied, ethoxyphenol (**1**, EP), 4-phenoxyphenol (**2**, PP), p-benzyloxyphenol (**3**, PBP) and 2-(2-phenylethoxy)phenol (**4**, 2-PEP), in the [BSO_3Hmim][OTf]-H_2O (2:1) electrolyte. It can be seen that no degradation reaction occurs in the absence of external conditions.

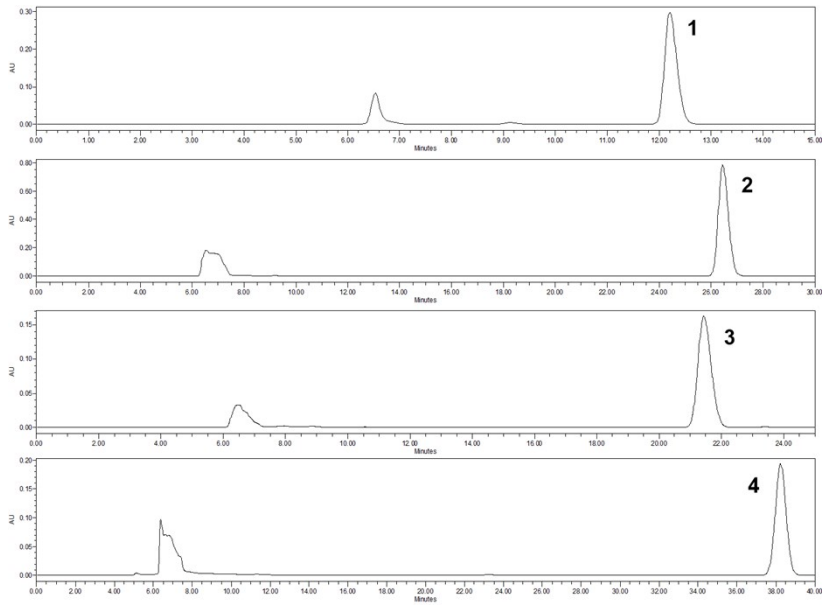

Fig S10. Chromatograms of [BSO_3Hmim][OTf]-H_2O (2:1) electrolyte containing 20 mM EP, PP, PBP and 2-PEP were determined by HPLC. Conditions: room temperature, reaction time 12 h, under air atmosphere.

11. Degradation products of PBP

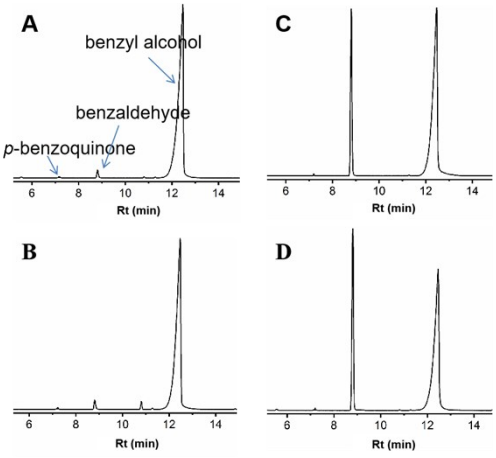

Fig S11. Gas chromatograms of PBP degradation products. Conditions: (A) and (B), RuO_2-IrO_2/Ti mesh electrode hold at 0.6 V; (C) and (D), graphite felt electrode hold at 0.6 V. Room temperature, reaction time 12 h, under both N_2 and O_2 atmosphere, respectively.

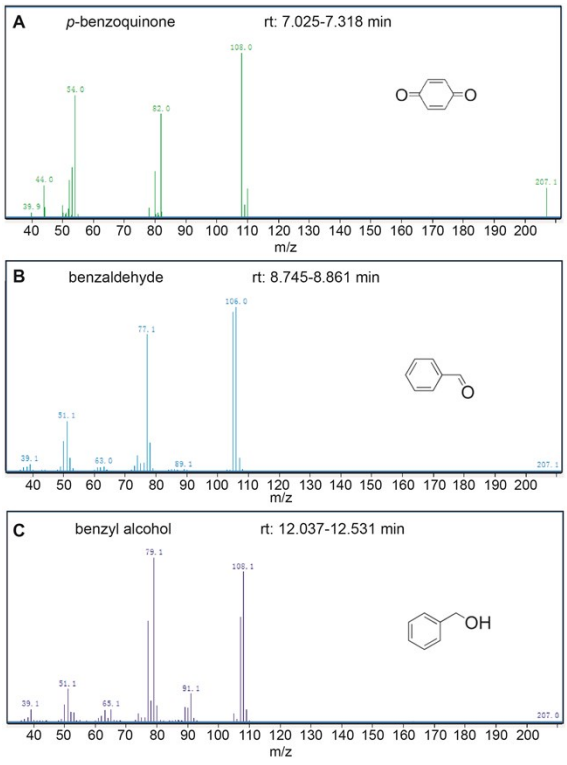

Fig S12. Mass spectra of PBP degradation products. (A), (B) and (C) are *p*-BQ, benzaldehyde, and benzyl alcohol, respectively.

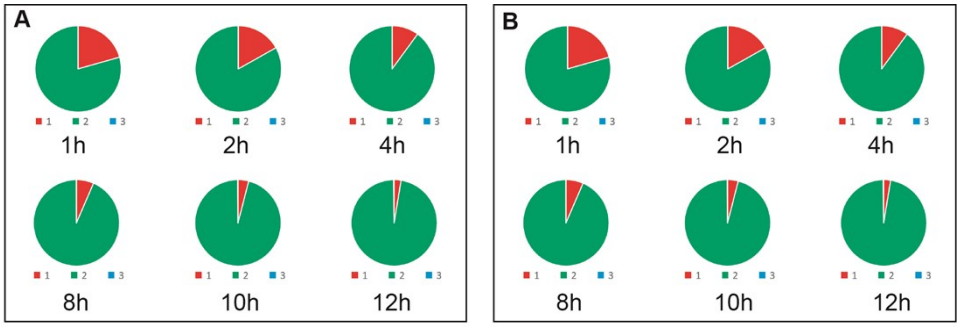

Fig S13. Products distribution at different times. Conditions: RuO_2-IrO_2/Ti mesh used as working electrode hold at 0.6 V, 20 mM PBP, room temperature, [BSO_3Hmim][OTf]-H_2O (2:1). (A) N_2 atmosphere, (B) O_2 atmosphere. 1, *p*-BQ; 2, benzyl alcohol; 3, benzaldehyde.

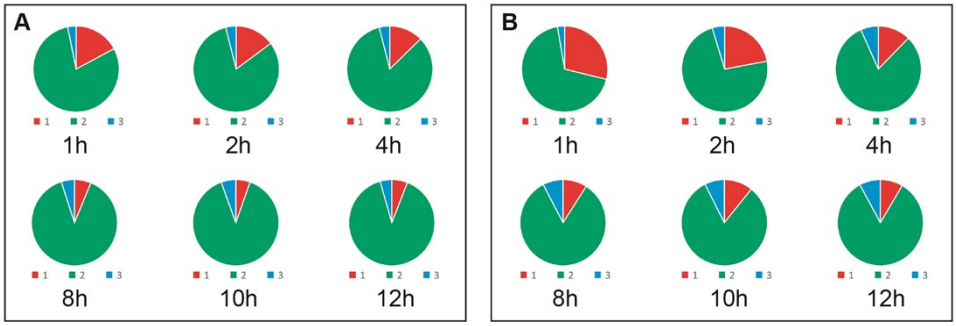

Fig S14. Products distribution at different times. Conditions: Graphite felt used as working electrode hold at 0.6 V, 20 mM PBP, room temperature, [BSO_3Hmim][OTf]-H_2O (2:1). (A) N_2 atmosphere, (B) O_2 atmosphere. 1, *p*-BQ; 2, benzyl alcohol; 3, benzaldehyde.

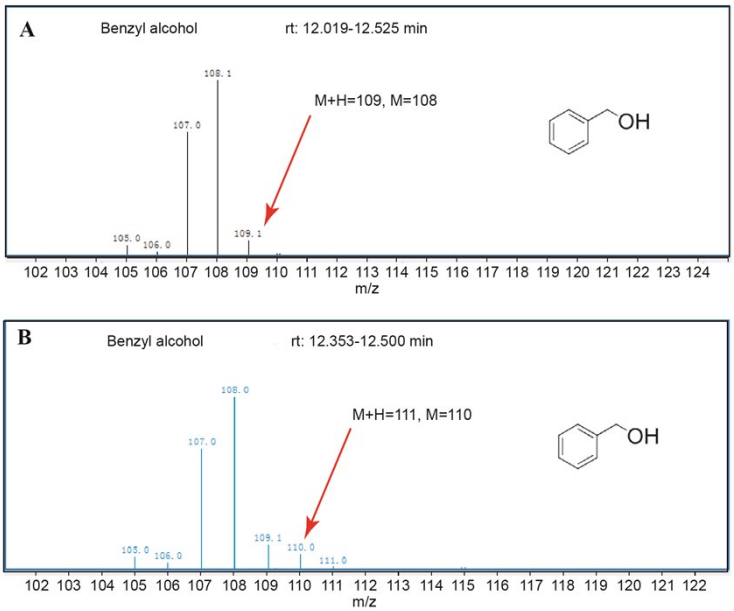

Fig S15. (A) Mass spectrum of benzyl alcohol with H_2O as hydroxyl donor. (B) Mass spectrum of benzyl alcohol with $H_2{}^{18}O$ as hydroxyl donor. Conditions: RuO_2-IrO_2/Ti mesh used as working electrode hold at 0.6 V, N_2 atmosphere, room temperature.

12. Degradation products of EP

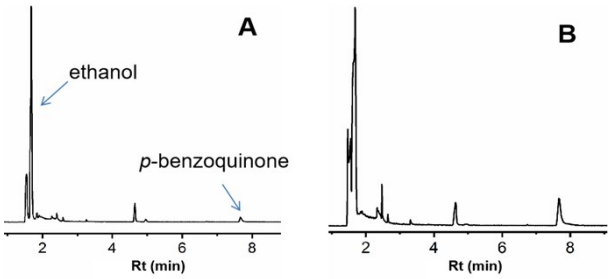

Fig S16. Gas chromatograms of EP degradation products. Conditions: RuO_2-IrO_2/Ti mesh electrode hold at 0.6 V, room temperature, reaction time 12 h, under both N_2 and O_2 atmosphere, respectively.

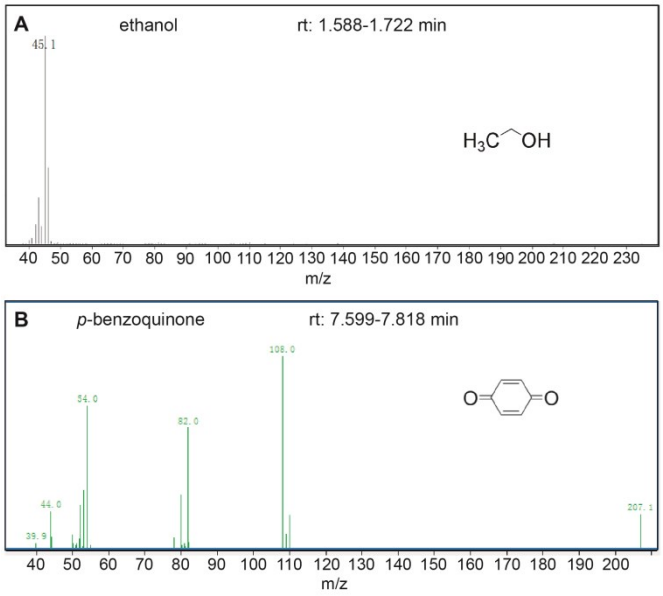

Fig S17. Mass spectra of EP degradation products. (A), ethanol; (B), *p*-BQ.

13. Possible electrochemical degradation mechanism of EP

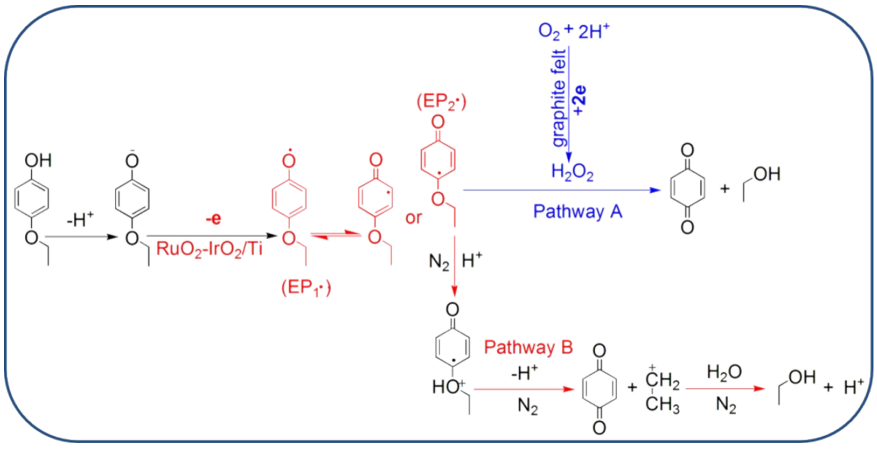

Scheme S3. Possible electrochemical degradation mechanism of EP in [BSO_3Hmim][OTf]-H_2O system *via* direct (Pathway B) and indirect oxidation (Pathway A).

14. Degradation products of PP

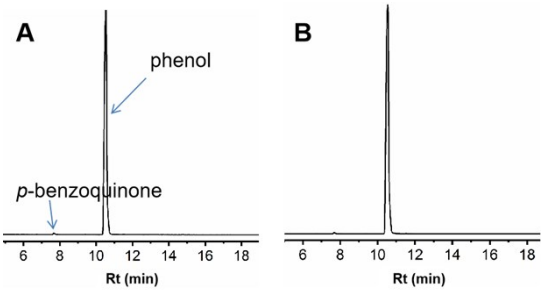

Fig S18. Gas chromatograms of PP degradation products. Conditions: RuO_2-IrO_2/Ti mesh electrode hold at 0.75 V, room temperature, reaction time 12 h, under both N_2 and O_2 atmosphere, respectively.

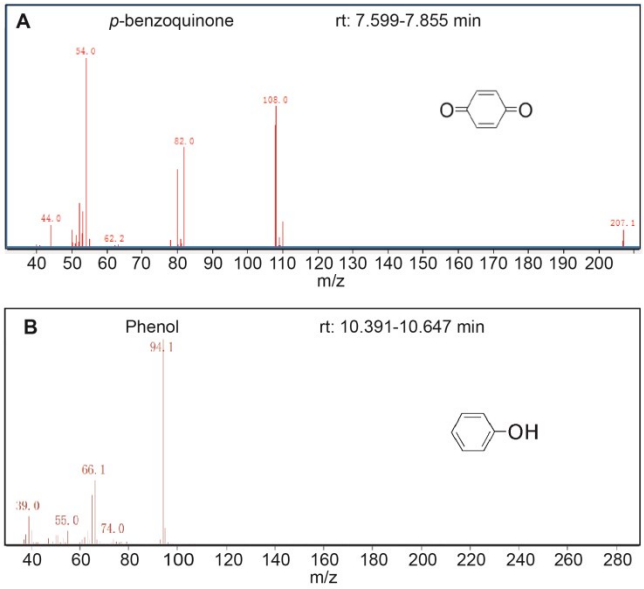

Fig S19. Mass spectra of PP degradation products. (A), *p*-BQ; (B), phenol.

15. Possible electrochemical degradation mechanism of PP

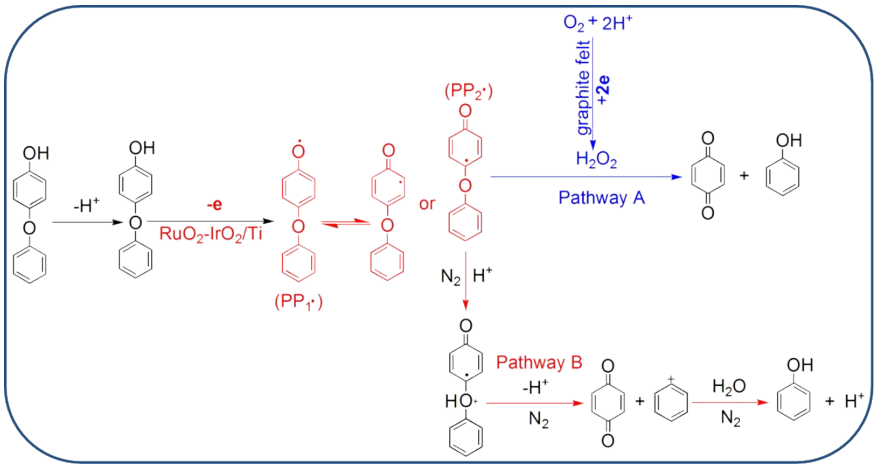

Scheme S4. Possible electrochemical degradation mechanism of PP in [BSO_3Hmim][OTf]-H_2O system *via* direct (Pathway B) and indirect oxidation (Pathway A).

16. Degradation products of 2-PEP

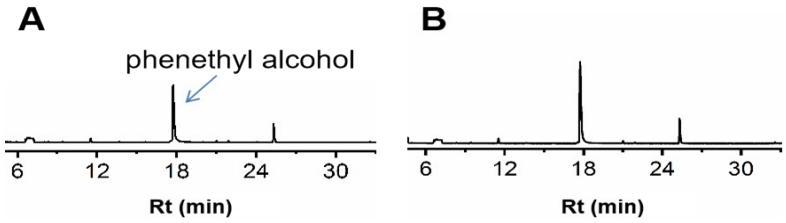

Fig S20. Gas chromatograms of 2-PEP degradation product. Conditions: RuO_2-IrO_2/Ti mesh electrode hold at 0.71 V, room temperature, reaction time 12 h, under both N_2 and O_2 atmosphere, respectively.

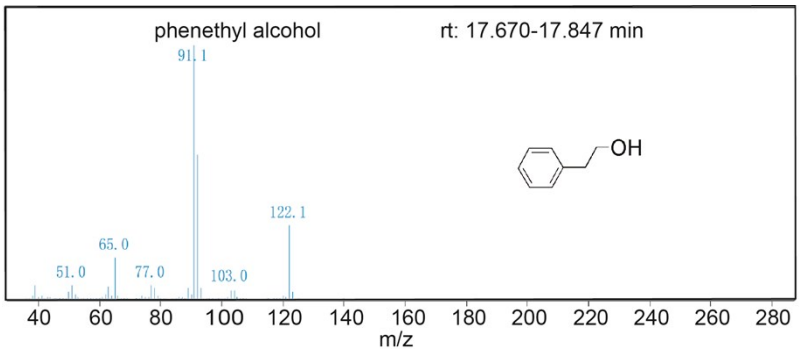

Fig S21. Mass spectrum of 2-PEP degradation product.

17. Possible electrochemical degradation mechanism of 2-PEP

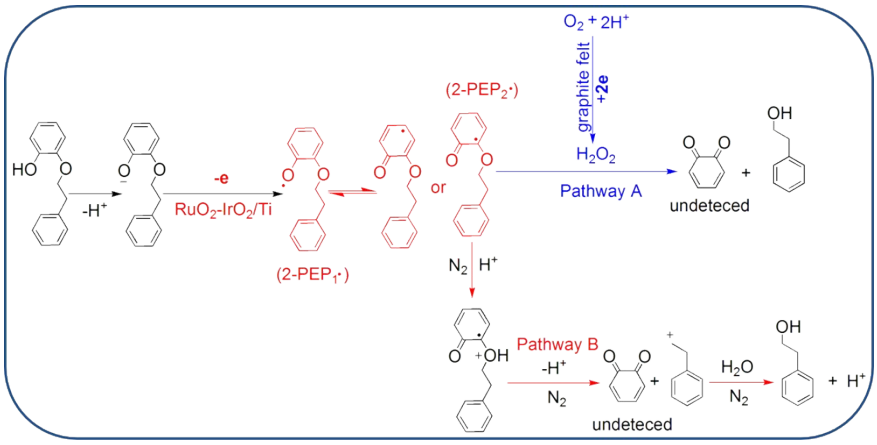

Scheme S5. Possible electrochemical degradation mechanism of 2-PEP in [BSO_3Hmim][OTf]-H_2O system *via* direct (Pathway B) and indirect oxidation (Pathway A).

References

1 S. Plimpton, *J. Comput. Phys*., 1995, **117**, 1-19.

2 J. N. C. Lopes and A. A. H. Padua, *J. Phys. Chem. B*, 2004, **108**, 16893-16898.

3 J. N. C. Lopes, A. A. H. Padua and K. Shimizu, *J. Phys. Chem. B*, 2008, **112**, 5039-5046.

4 J. N. C. Lopes, J. Deschamps and A. A. H. Padua, *J. Phys. Chem. B*, 2004, **108**, 2038-2047.

239 5 C. Qian, B. Ding, Z. W. Wu, W. L. Ding, F. Huo, H. Y. He, N. Wei, Y. L. Wang and X. P. Zhang,
240 *Ind. Eng. Chem. Res*., 2019, **58**, 20109-20115.

241 6 C. L. Wang, Y. L. Wang, Y. M. Lu, H. Y. He, F. Huo, K. Dong, N. Wei and S. J. Zhang, *Phys. Chem.*
242 *Chem. Phys*., 2019, **21**, 12767-12776.

243 7 Y. L. Wang, C. L. Wang, Y. Q. Zhang, F. Huo, H. Y. He and S. J. Zhang, *Small*, 2019, **15**, 10.

244 8 H. J. C. Berendsen, J. R. Grigera and T. P. Straatsma, *J. Phys. Chem*., 1987, **91**, 6269-6271.

245 9 J. P. Ryckaert, G. Ciccotti and H. J. C. Berendsen, *J. Comput. Phys*., 1977, **23**, 327-341.

246 10 N. Hansen, F. A. B. Agbor and F. J. Keil, *Fluid Phase Equilibr*., 2007, **259**, 180-188.

247 11 H. J. C. Berendsen, J. P. M. Postma, J. P. M. van Gunsteren, A. DiNola and J. R. Haak, *J. Chem.*
248 *Phys*., 1984, **81**, 3684-3690.

249 12 L. Ma, Z. Wang and Q. Li, *Analyst*, 2012, **137**, 432-436.

250 13 T. A. Enache and A. M. Oliveira-Brett, *J. Electroanal. Chem.*, 2011, **655**, 9-16.

251 14 L. Wang, S. Liu, H. Jiang, Y. Chen, L. Wang, G. Duan, Y. Sun, Y. Chen and P. Wan, *J. Electrochem.*
252 *Soc.*, 2018, **165**, H705-H710.